



Test of lepton flavour universality with $B_s^0 \rightarrow \phi \ell^+ \ell^-$ decays

LHCb collaboration[†]

Abstract

Lepton flavour universality in rare $b \rightarrow s$ transitions is tested for the first time using B_s^0 meson decays. The measurements are performed using pp collision data collected by the LHCb experiment between 2011 and 2018, corresponding to a total integrated luminosity of 9 fb^{-1} . Branching fraction ratios between the $B_s^0 \rightarrow \phi e^+ e^-$ and $B_s^0 \rightarrow \phi \mu^+ \mu^-$ decays are measured in three regions of dilepton mass squared, q^2 , with $0.1 < q^2 < 1.1$, $1.1 < q^2 < 6.0$, and $15 < q^2 < 19 \text{ GeV}^2/c^4$. The results agree with the Standard Model expectation of lepton flavour universality.

Submitted to Phys. Rev. Lett.

© 2024 CERN for the benefit of the LHCb collaboration. [CC BY 4.0 licence](#).

[†]Authors are listed at the end of this letter.

The decay of a B_s^0 meson to a ϕ meson and pair of oppositely charged leptons, $\ell^+\ell^-$, involves a b - to s -quark flavour-changing neutral-current transition. Such processes are rare in the Standard Model of particle physics (SM). In extensions of the SM, the rates of these processes could be modified by the contribution of as-yet undiscovered particles. The branching fraction of the $B_s^0 \rightarrow \phi\mu^+\mu^-$ decay, $\mathcal{B}(B_s^0 \rightarrow \phi\mu^+\mu^-)$, has been measured by the CDF [1] and LHCb [2–4] collaborations as a function of the dilepton mass squared, q^2 . The experimental measurements are systematically below theoretical predictions, with a local tension as large as 3.6 standard deviations [4]. However, comparisons with theoretical predictions are complicated by sizeable uncertainties on the form factors for the $B_s^0 \rightarrow \phi$ transition [5, 6] and hadronic corrections to the decay rate [7, 8]. Discrepancies with SM predictions have also been found in the angular distributions of the $B_s^0 \rightarrow \phi\mu^+\mu^-$ decay [9], as well as in the rate and angular distribution of other $b \rightarrow s\mu^+\mu^-$ transitions [10–18]. This pattern of tensions with SM predictions has led to significant discussion within the community [19–34].

Lepton flavour universality tests, which compare the rates of processes involving different flavours of charged leptons, can provide powerful probes of the SM. In such comparisons, SM uncertainties associated with hadronic form factors largely cancel and, since the electroweak couplings are flavour-universal, processes are expected to differ only by phase-space and QED effects [35, 36]. In some extensions of the SM, this accidental flavour-symmetry could be violated (see for example Refs. [37–40]).

In this Letter, a first measurement of the lepton universality ratio $R_\phi = \mathcal{B}(B_s^0 \rightarrow \phi\mu^+\mu^-)/\mathcal{B}(B_s^0 \rightarrow \phi e^+e^-)$ is reported. Inclusion of charge-conjugate processes is implied throughout. The analysis uses data from pp collisions at centre-of-mass energies of $\sqrt{s} = 7, 8, \text{ and } 13$ TeV, corresponding to a total integrated luminosity of 9 fb^{-1} , collected by the LHCb collaboration between 2011 and 2018. Measurements are performed in three bins of q^2 : $0.1 < q^2 < 1.1$ (low), $1.1 < q^2 < 6.0$ (central), and $15 < q^2 < 19 \text{ GeV}^2/c^4$ (high). The lowest q^2 bin contains small contributions from light-quark resonances decaying to $\ell^+\ell^-$ (predominantly the $\rho(770)^0$ and ϕ mesons). Similar tests involving $B^{\{+,0\}} \rightarrow K^{\{+,0\}}\ell^+\ell^-$, $B^{\{+,0\}} \rightarrow K^{*\{+,0\}}\ell^+\ell^-$ and $\Lambda_b^0 \rightarrow pK^-\ell^+\ell^-$ decays have previously been performed by the BaBar [41], Belle [42], CMS [17] and LHCb collaborations [43–49]. One advantage of performing tests with $B_s^0 \rightarrow \phi\ell^+\ell^-$ decays is that the clean signature of the $\phi \rightarrow K^+K^-$ decay significantly reduces most sources of background. This facilitates the inclusion of the high- q^2 bin, which has not been studied in previous LHCb publications.

The analysis strategy follows closely the approach described in Refs. [48, 49]. To reduce systematic uncertainties on the modelling of the lepton reconstruction efficiency, the double ratio of branching fractions,

$$R_\phi = \left(\frac{\mathcal{B}(B_s^0 \rightarrow \phi\mu^+\mu^-)}{\mathcal{B}(B_s^0 \rightarrow J/\psi(\rightarrow \mu^+\mu^-)\phi)} \right) / \left(\frac{\mathcal{B}(B_s^0 \rightarrow \phi e^+e^-)}{\mathcal{B}(B_s^0 \rightarrow J/\psi(\rightarrow e^+e^-)\phi)} \right), \quad (1)$$

is measured. Here, each individual branching fraction is obtained as the corresponding yield in the relevant q^2 interval divided by its efficiency, with other multiplicative factors that cancel exactly in Eq. (1). In practice, R_ϕ^{-1} is measured rather than R_ϕ such that the small $B_s^0 \rightarrow \phi e^+e^-$ yield appears in the numerator and the statistical behaviour of the observable more closely follows a Gaussian distribution. To avoid experimenter’s bias, the $B_s^0 \rightarrow \phi e^+e^-$ candidates with masses in the range $5.2\text{--}5.5 \text{ GeV}/c^2$ (slightly different for each q^2 interval), the corresponding signal yields, and R_ϕ^{-1} are not inspected until all aspects of the analysis procedure are finalised.

The LHCb detector [50, 51] is a single-arm forward spectrometer covering the pseudorapidity range $2 < \eta < 5$, designed for the study of particles containing b or c quarks. The detector includes a high-precision tracking system, comprising silicon-strip [52, 53] and straw drift-tube [54] detectors. Different types of charged hadrons are distinguished using information from two ring-imaging Cherenkov detectors [55]. Electrons are identified using a calorimeter system comprising scintillating-pad and preshower detectors, an electromagnetic, and a hadronic calorimeter. Muons are identified by a system composed of alternating layers of iron and multiwire proportional chambers [56]. The online event selection is performed by a trigger [57], which consists of a hardware and a software stage.

Simulated data samples are used to determine the efficiency of the event reconstruction and candidate selection, which is needed to determine the branching fractions from the observed yields. These samples are also used to understand candidate mass lineshapes, and the contributions from different background sources. In the simulation, pp collisions are generated using PYTHIA [58] with a specific LHCb configuration [59]. Decays of unstable particles are described by EVTGEN [60], in which final-state radiation is generated using PHOTOS [61]. Simulated $B_s^0 \rightarrow \phi \ell^+ \ell^-$ decays are generated according to a model based on Refs. [62–64]. The interactions of the generated particles with the detector, and its response, are simulated using the GEANT4 toolkit [65] as described in Ref. [66]. The simulated samples are corrected to account for known data-simulation differences in the B_s^0 production kinematics and detector occupancy, as well as track reconstruction, particle identification and trigger efficiencies. The q^2 distribution of the simulated $B_s^0 \rightarrow \phi e^+ e^-$ sample is smeared to better match the resolution of the $B_s^0 \rightarrow J/\psi \phi$ candidates in data.

The analysis uses data triggered at the hardware stage either by particles in the event that are not used to form signal candidates, or by an electron (muon) with large transverse energy (transverse momentum) for $B_s^0 \rightarrow \phi e^+ e^-$ ($B_s^0 \rightarrow \phi \mu^+ \mu^-$) decays. The E_T (p_T) thresholds vary in the ranges 2.4–3.0 GeV (1.5–2.9 GeV/ c). In the subsequent software trigger, events are retained if they contain at least one reconstructed track that has a large p_T and is significantly displaced from every primary proton-proton interaction vertex (PV). This track is then combined with at least one other track to form a vertex and events are retained based on topological criteria [67, 68]. Offline, $B_s^0 \rightarrow \phi \ell^+ \ell^-$ candidates are formed by combining two leptons of opposite charge with a pair of kaons of opposite charge. A dedicated algorithm is used to correct for the bremsstrahlung emission of the electrons, associating energy deposits in the calorimeter to electrons based on their trajectories. Candidates are accepted if their reconstructed mass is in the range $5000 < m(K^+ K^- \mu^+ \mu^-) < 6000$ or $4600 < m(K^+ K^- e^+ e^-) < 6600$ MeV/ c^2 and if the kaon pair has a mass within ± 12 MeV/ c^2 of the known ϕ meson mass [69]. Contributions in this mass region from $B_s^0 \rightarrow K^+ K^- \ell^+ \ell^-$ decays, where the kaons do not originate from a ϕ meson, are known to be small and are neglected [4]. The leptons and kaons must have significant impact parameter (IP) values and form a common vertex that is displaced from every PV. The B_s^0 candidate is required to have a small IP with respect to one of the PVs and have its momentum aligned with the displacement vector from that PV. In the $B_s^0 \rightarrow \phi \mu^+ \mu^-$ sample, candidates with dimuon masses within ± 100 MeV/ c^2 of the known J/ψ mass are assumed to originate from $B_s^0 \rightarrow J/\psi \phi$ decays. A wider range, $6 < q^2 < 11$ GeV $^2/c^4$, is used for $B_s^0 \rightarrow J/\psi(\rightarrow e^+ e^-) \phi$ decays to account for the worse mass resolution resulting from bremsstrahlung and the associated energy recovery procedure.

Combinatorial backgrounds are suppressed using a gradient boosted decision tree (BDT)

classifier [70]. The classifier uses topological and kinematic information, including: the chi-square of a common vertex fit to the four particles, the consistency of the B_s^0 candidate with originating from a PV, the displacement of the candidate's decay vertex from that PV, its p_T , and the p_T and IP of the kaons and the leptons. Separate classifiers are trained for the dielectron and dimuon final states and for the 2011–2012, 2015–2016 and 2017–2018 run periods. Simulated signal decays and candidates from upper mass sidebands, with $m(K^+K^-\mu^+\mu^-) > 5400$ and $m(K^+K^-e^+e^-) > 5600 \text{ MeV}/c^2$, are used as signal and background proxies in the training. To increase the amount of data available for training and avoid biases, k -fold cross-validation [71] with $k = 10$ is used for the training/testing samples. The working points of the classifier are chosen to optimise the precision on an R_ϕ measurement based on the measured $B_s^0 \rightarrow \phi\mu^+\mu^-$ branching fraction [4], assuming $R_\phi = 1$. Working points are optimised separately for the three q^2 regions.

The narrow window around the ϕ meson mass reduces the background from many specific b -hadron decays. Backgrounds from $B^0 \rightarrow K^{*0}(\rightarrow K^+\pi^-)\ell^+\ell^-$ and $\Lambda_b^0 \rightarrow pK^-\ell^+\ell^-$ decays are reduced to a negligible level by particle identification requirements. Potential background from $B_s^0 \rightarrow D_s^-(\rightarrow \phi\pi^-)\ell^+\nu_\ell$ decays, where the π^- is mistakenly identified as a lepton, is rejected by removing candidates if the $\phi\ell^-$ mass is consistent with that of a D_s^- meson after the pion mass has been assigned to the lepton. Additional particle identification criteria are applied to remove b -hadron decays to J/ψ or $\psi(2S)$ mesons and two charged hadrons, where a hadron is mistakenly reconstructed as a lepton and vice versa. These criteria are applied for $B_s^0 \rightarrow \phi\mu^+\mu^-$ candidates if the mass formed by the hadron and muon of opposite charge is consistent with the J/ψ or $\psi(2S)$ mass when the hadron is assigned the muon mass. For $B_s^0 \rightarrow \phi e^+e^-$ candidates the criteria are applied if the four-body mass, calculated with the electron mass assigned to the K^\pm , and the e^\pm assigned either the pion, kaon or proton mass, is close to that of a known b -hadron.

The $\phi\ell^+\ell^-$ final state has relatively few potential backgrounds from partially reconstructed b -hadron decays with missing hadrons. The most relevant are $B^{\{0,+ \}} \rightarrow \phi K^{\{0,+ \}}\ell^+\ell^-$ decays where the kaon is not reconstructed. Backgrounds from hadronic b decays, where two charged hadrons are misidentified as leptons and potentially one or more hadrons are not reconstructed, are poorly known. The contribution from these backgrounds is estimated using the same data-driven approach as employed in Refs. [48, 49].

A separate BDT classifier is trained to reject background in the high- q^2 interval from $J/\psi \rightarrow e^+e^-$ decays originating from a b -hadron, where bremsstrahlung photons have been incorrectly assigned to the electrons, or incorrectly reconstructed. The BDT classifier is trained using simulated events and uses information on the bremsstrahlung photon energy, reconstructed track momentum, track asymmetries and the dielectron mass.

After applying the full selection less than 0.3% of events contain more than one candidate, in which case a single candidate is selected at random. The yields of $B_s^0 \rightarrow \phi\ell^+\ell^-$ and $B_s^0 \rightarrow J/\psi\phi$ decays are determined by performing unbinned extended maximum-likelihood fits to the mass distributions of the candidates in the different samples, using ZFIT [72]. The fit is performed simultaneously, where R_ϕ^{-1} is shared over the different data-taking periods. The $B_s^0 \rightarrow \phi\ell^+\ell^-$ and $B_s^0 \rightarrow J/\psi\phi$ signals are described by modified Gaussian functions with power-law tails. The functions have different width and tail parameters on the left- and right-hand sides of the distribution. For $B_s^0 \rightarrow \phi e^+e^-$ decays, the lineshape is obtained by summing functions that represent the cases where either zero, one, or two or more calorimeter clusters are associated with bremsstrahlung from the

dielectron pair. The fractional contribution of these functions is fixed from simulation, together with the tail parameters of the signal shapes. The peak and width parameters for each q^2 bin are taken from simulation but are allowed to vary by scale factors in the fits to the data. For the $B_s^0 \rightarrow \phi \ell^+ \ell^-$ samples, the scale factors are constrained to match those of the corresponding $B_s^0 \rightarrow J/\psi \phi$ samples.

Combinatorial background in the low- and central- q^2 bins is described by an exponential function. The combinatorial shape is modified at high q^2 , by multiplying the exponential function by a sigmoid function to account for the reduced q^2 range available at low $m(K^+ K^- \ell^+ \ell^-)$. The shape of the sigmoid is determined from a model where $m(K^+ K^- \ell^+ \ell^-)$ and q^2 are described by exponential functions, which are parameterised using candidates at large $m(K^+ K^- \ell^+ \ell^-)$. It is verified with data that there is negligible correlation between the q^2 and $m(K^+ K^- \ell^+ \ell^-)$ distributions.

Background from semileptonic decays of a B_s^0 to a D_s^- meson, where the D_s^- also decays semileptonically, is modelled by an exponential function with a slope parameter fixed from simulation. This background is only present in the low- and central- q^2 bins. The shape and level of background from misidentified hadrons are obtained by combining three control regions in data, where either one or both leptons are selected with particle identification criteria favouring hadrons, following the procedure in Refs. [48, 49].

For the fit to the dielectron samples, additional background components, with parameters fixed from simulation, are included to account for leakage from $B_s^0 \rightarrow J/\psi \phi$ ($B_s^0 \rightarrow \psi(2S)\phi$) decays into the central- and high- q^2 (high- q^2 only) bins. In central q^2 , the $B_s^0 \rightarrow J/\psi \phi$ leakage is described by a Gaussian function. At high q^2 , the $B_s^0 \rightarrow J/\psi \phi$ and $B_s^0 \rightarrow \psi(2S)\phi$ leakage shapes are described by a nonparametric kernel density estimate and by a Johnson S_U function [73], respectively. For the $B_s^0 \rightarrow J/\psi \phi$ samples, background components are included to describe $B^0 \rightarrow J/\psi K^{*0}$ and $\Lambda_b^0 \rightarrow J/\psi p K^-$ decays. These components are taken nonparametrically from simulated samples. The yields of semileptonic, leakage and misidentified backgrounds are each constrained in the fits to estimates from simulation.

Figure 1 shows the mass distributions of selected $B_s^0 \rightarrow \phi e^+ e^-$ candidates in the different q^2 bins. The corresponding mass distributions for selected $B_s^0 \rightarrow \phi \mu^+ \mu^-$ candidates, which are similar to those in Ref. [4], are provided as supplemental material. The yields of the $B_s^0 \rightarrow \phi e^+ e^-$ ($B_s^0 \rightarrow \phi \mu^+ \mu^-$) decays in the low-, central-, and high- q^2 bin are 63 ± 9 (159 ± 13), 119 ± 14 (300 ± 18) and 50 ± 13 (312 ± 18), respectively. The lower yield for the dielectron- compared to the dimuon-modes is due to lower track-reconstruction efficiency for electrons and the large E_T requirement necessary to select them in the hardware trigger. The statistical significance of the $B_s^0 \rightarrow \phi e^+ e^-$ signal in the three q^2 bins is determined using Wilks' theorem [74] to correspond to 6.8, 5.4 and 3.6 standard deviations (σ).

The analysis is validated using pseudoexperiments, generated with $R_\phi = 1$ and taking $\mathcal{B}(B_s^0 \rightarrow \phi \mu^+ \mu^-)$ from Ref. [4]. The resulting fits are found to have good coverage and little bias. The bias is corrected and the uncertainty on the bias assigned as a source of systematic uncertainty. Several cross-checks are performed to validate the analysis using data. The branching fraction of the $B_s^0 \rightarrow \phi \mu^+ \mu^-$ decay is measured and found to be consistent with Ref. [4]. Consistent values of R_ϕ^{-1} are found when analysing the data with stricter particle identification requirements. The $B_s^0 \rightarrow J/\psi \phi$ yields are also determined from fits to the candidate mass distribution with the $\ell^+ \ell^-$ mass constrained to the known mass of the J/ψ meson. This significantly improves the mass resolution on the $B_s^0 \rightarrow J/\psi \phi$

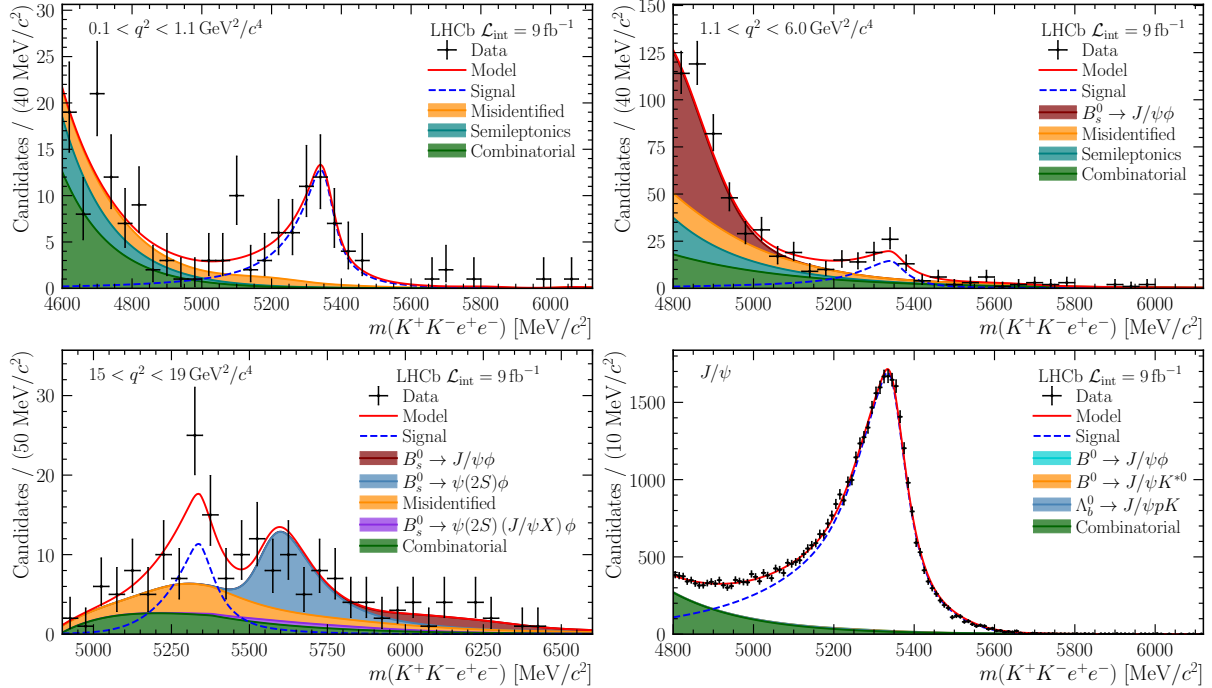


Figure 1: Mass distributions of selected $B_s^0 \rightarrow \phi e^+ e^-$ candidates in the (top left) low-, (top right) central-, (bottom left) high- q^2 , and (bottom right) J/ψ bins. The data are summed over the three data-taking periods and are compared with the result of the fit described in the text.

samples but only changes the yields by 0.2%, confirming that the $K^+ K^- \ell^+ \ell^-$ mass model gives an appropriate description of the data. The ratio of branching fractions between $B_s^0 \rightarrow J/\psi(\rightarrow \mu^+ \mu^-) \phi$ and $B_s^0 \rightarrow J/\psi(\rightarrow e^+ e^-) \phi$ decays, $r_{J/\psi}$, is determined from fits to the constrained masses, in bins of different kinematic variables, and found to be consistent with unity; the most significant variation is used to assign a systematic uncertainty on the measurement. The value of $r_{J/\psi}$ for the combined data set is $r_{J/\psi} = 0.997 \pm 0.013$, where the uncertainty combines the statistical and a subset of the systematic uncertainties pertaining to the limited size of the calibration samples used in the data-simulation corrections. The double ratio $R_{\psi(2S)}$, defined by replacing the signal mode $B_s^0 \rightarrow \phi \ell^+ \ell^-$ with the decay $B_s^0 \rightarrow \psi(2S) \phi$ in Eq. 1, is determined from fits to candidates with $11 < q^2 < 15 \text{ GeV}^2/c^4$. The double ratio is found to be $R_{\psi(2S)} = 1.010 \pm 0.026$, consistent with the expectation of unity, where again the uncertainty combines statistical and systematic contributions. An independent test [75] using ϕ mesons from D_s^+ decays, that decay to $e^+ e^-$ and $\mu^+ \mu^-$, shows that the lepton efficiency is well understood even for lower momentum leptons.

The different sources of systematic uncertainty on R_ϕ^{-1} considered in the analysis are summarised in Table 1. Sources of uncertainty on the efficiencies, related to the finite size of the simulation and variations of the data-simulation corrections, impact R_ϕ^{-1} at the $\sim 1\%$ level. Small variations of the decay model used in the simulation, accounting for the time dependence of the signal decay rate, have a minimal impact on R_ϕ^{-1} . Variations of the q^2 resolution also impact the efficiency calculation as simulated decays migrate into and out of the q^2 bins used in the analysis. A systematic uncertainty on the q^2 -resolution correction is determined by evaluating separate correction factors from the $B_s^0 \rightarrow J/\psi \phi$ sample in bins of electron p_T . Modifying the correction factors changes R_ϕ^{-1} by less than

Table 1: Sources of systematic uncertainty in 10^{-2} on the R_ϕ^{-1} measurement in the low-, central- and high- q^2 bins. The total uncertainty is computed by combining the contributions from individual sources in quadrature.

Source	low	central	high
Fit bias	<0.1	0.9	1.4
Normalisation	0.2	0.2	0.2
$r_{J/\psi}$ variation	1.3	0.6	0.9
Efficiency calibration	0.7	0.5	1.2
q^2 smearing	0.6	0.5	0.3
Decay model	0.1	0.3	0.1
Signal lineshape	1.7	1.5	3.7
Misidentified bkg.	4.1	4.3	7.4
Combinatorial bkg.	–	–	3.9
Leakage bkg.	–	0.9	2.1
Semileptonic bkg.	1.3	1.2	–
Total	4.9	4.9	9.6

1%.

The largest sources of systematic uncertainty are associated with the modelling of the signal and background in the likelihood fits. The uncertainty associated with the signal lineshape is estimated by replacing the model by a simplified function, with a single Gaussian core, and by varying the fractions of the different bremsstrahlung categories that form the lineshape. The uncertainty on the modelling of misidentified hadronic backgrounds is determined by varying both the size and shape of the contribution in the fit. Variations are made to the particle-identification requirements used to define the background-like control regions, the efficiency maps that translate yields in the background-like regions to yields in the signal region, and in the model used to parameterise the lineshape. The effect of the finite size of the background-like samples is assessed using a bootstrapping technique [76]. Uncertainty on the high- q^2 combinatorial-background shape is evaluated by varying the shape of the q^2 distribution used to determine the sigmoid parameters, and by replacing the model by an alternate function with a power-law turn-on and exponential fall-off, with parameters constrained from a fit to data with same-sign $\ell^\pm\ell^\pm$ or $K^\pm K^\pm$ combinations. An uncertainty from the J/ψ and $\psi(2S)$ leakage into the central- and high- q^2 bins is assigned by replacing the parametric shapes by a nonparametric model, varying the constraints on the background yields in the fit, and by varying the q^2 resolution in the simulation. An uncertainty associated with the semileptonic background is evaluated by estimating the effects of replacing the background model by a nonparametric model and varying the background level.

The R_ϕ^{-1} values in the three q^2 ranges are given in Table 2. The results are in good agreement with the SM expectation. Figure 2 shows the variation with R_ϕ^{-1} of the difference in log-likelihood of the fit from the best fit point. For low q^2 , a local minimum around $R_\phi^{-1} \sim 1.3$ yields a nonparabolic profile likelihood towards lower R_ϕ^{-1} values. The presence of this additional minimum is evident when considering the variation of the likelihood in the full parameter space. The 2σ interval on R_ϕ^{-1} from the profile likelihood

Table 2: Values of R_ϕ^{-1} and $d\mathcal{B}(B_s^0 \rightarrow \phi e^+ e^-)/dq^2$ in the low-, central- and high- q^2 bins. The first uncertainty is statistical and the second systematic. For the differential branching fraction, the third and the fourth uncertainty are due to the experimental uncertainty on the ratio $d\mathcal{B}(B_s^0 \rightarrow \phi \mu^+ \mu^-)/dq^2/\mathcal{B}(B_s^0 \rightarrow J/\psi \phi)$ [4] and on $\mathcal{B}(B_s^0 \rightarrow J/\psi \phi)$ [69, 78], respectively.

q^2 [GeV $^2/c^4$]	R_ϕ^{-1}	$d\mathcal{B}(B_s^0 \rightarrow \phi e^+ e^-)/dq^2$ [10^{-7} GeV $^{-2}c^4$]
$0.1 < q^2 < 1.1$	$1.57^{+0.28}_{-0.25} \pm 0.05$	$1.38^{+0.25}_{-0.22} \pm 0.04 \pm 0.19 \pm 0.06$
$1.1 < q^2 < 6.0$	$0.91^{+0.20}_{-0.19} \pm 0.05$	$0.26 \pm 0.06 \pm 0.01 \pm 0.01 \pm 0.01$
$15.0 < q^2 < 19.0$	$0.85^{+0.24}_{-0.23} \pm 0.10$	$0.39 \pm 0.11 \pm 0.04 \pm 0.02 \pm 0.02$

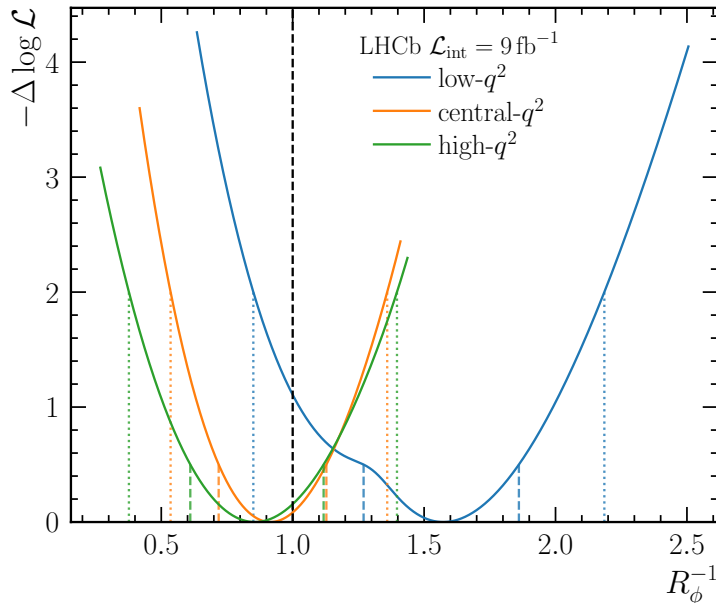


Figure 2: Profile log-likelihood of R_ϕ^{-1} for the low-, central- and high- q^2 bins, relative to the best fit point. Systematic uncertainties are included by convolving the likelihood from the fit with a Gaussian distribution of width equal to the systematic uncertainty. The vertical lines indicate the 1 and 2 σ confidence intervals, respectively.

is [0.86, 2.18], in agreement at the level of 1.4 σ with a SM prediction of 1.016 computed using Ref. [77]. Depending on the $m(K^+ K^- e^+ e^-)$ mass range, the particle identification criteria and BDT requirement, the minimum at $R_\phi^{-1} \sim 1.3$ can be favoured. Table 2 also presents the differential branching fraction of the $B_s^0 \rightarrow \phi e^+ e^-$ decay, determined from R_ϕ^{-1} , $d\mathcal{B}(B_s^0 \rightarrow \phi \mu^+ \mu^-)/dq^2/\mathcal{B}(B_s^0 \rightarrow J/\psi \phi)$ [4] and $\mathcal{B}(B_s^0 \rightarrow J/\psi \phi)$ [69, 78]. The upper value of the low- q^2 range in Ref. [4] is extrapolated from 0.98 GeV $^2/c^4$ to 1.1 GeV $^2/c^4$ by assuming that $d\mathcal{B}(B_s^0 \rightarrow \phi \mu^+ \mu^-)/dq^2$ is uniform in q^2 . At 2 σ , $d\mathcal{B}(B_s^0 \rightarrow \phi e^+ e^-)/dq^2$ in the low- q^2 region is in the range $[0.65, 2.08] \times 10^{-7}$ GeV $^{-2}c^4$. As implied by R_ϕ^{-1} , the $B_s^0 \rightarrow \phi e^+ e^-$ branching fraction is consistent with that of the $B_s^0 \rightarrow \phi \mu^+ \mu^-$ decay and lies below the central value of the SM prediction in the central- and high- q^2 bins.

In summary, the first measurement of the ratio of $B_s^0 \rightarrow \phi e^+ e^-$ and $B_s^0 \rightarrow \phi \mu^+ \mu^-$ branching fractions is presented. This represents the first test of lepton flavour universality with $B_s^0 \rightarrow \phi \ell^+ \ell^-$ decays. It is also the most precise test of lepton flavour universality in

the high- q^2 region of any measurement involving $b \rightarrow s\ell^+\ell^-$ transitions. Together with Ref. [79], this result constitutes the first observation of the $B_s^0 \rightarrow \phi e^+e^-$ decay. In addition, the differential branching fraction of the $B_s^0 \rightarrow \phi e^+e^-$ decay is measured in three bins of q^2 . The results are statistically limited and agree with the SM expectation of lepton flavour universality, placing important constraints on extensions of the SM.

Acknowledgements

We express our gratitude to our colleagues in the CERN accelerator departments for the excellent performance of the LHC. We thank the technical and administrative staff at the LHCb institutes. We acknowledge support from CERN and from the national agencies: CAPES, CNPq, FAPERJ and FINEP (Brazil); MOST and NSFC (China); CNRS/IN2P3 (France); BMBF, DFG and MPG (Germany); INFN (Italy); NWO (Netherlands); MNiSW and NCN (Poland); MCID/IFA (Romania); MICIU and AEI (Spain); SNSF and SER (Switzerland); NASU (Ukraine); STFC (United Kingdom); DOE NP and NSF (USA). We acknowledge the computing resources that are provided by CERN, IN2P3 (France), KIT and DESY (Germany), INFN (Italy), SURF (Netherlands), PIC (Spain), GridPP (United Kingdom), CSCS (Switzerland), IFIN-HH (Romania), CBPF (Brazil), and Polish WLCG (Poland). We are indebted to the communities behind the multiple open-source software packages on which we depend. Individual groups or members have received support from ARC and ARDC (Australia); Key Research Program of Frontier Sciences of CAS, CAS PIFI, CAS CCEPP, Fundamental Research Funds for the Central Universities, and Sci. & Tech. Program of Guangzhou (China); Minciencias (Colombia); EPLANET, Marie Skłodowska-Curie Actions, ERC and NextGenerationEU (European Union); A*MIDEX, ANR, IPhU and Labex P2IO, and Région Auvergne-Rhône-Alpes (France); AvH Foundation (Germany); ICSC (Italy); Severo Ochoa and María de Maeztu Units of Excellence, GVA, XuntaGal, GENCAT, InTalent-Inditex and Prog. Atracción Talento CM (Spain); SRC (Sweden); the Leverhulme Trust, the Royal Society and UKRI (United Kingdom).

Appendices

A Mass fits for $B_s^0 \rightarrow \phi\mu^+\mu^-$ decays

Figure 3 shows the mass distributions of selected $B_s^0 \rightarrow \phi\mu^+\mu^-$ candidates in the different q^2 bins. The significant difference in mass resolution between $B_s^0 \rightarrow \phi\mu^+\mu^-$ and $B_s^0 \rightarrow \phi e^+e^-$ decays, where the latter is shown in Fig. 1 in the Letter, is due to bremsstrahlung from the e^\pm and the imperfect nature of the bremsstrahlung recovery.

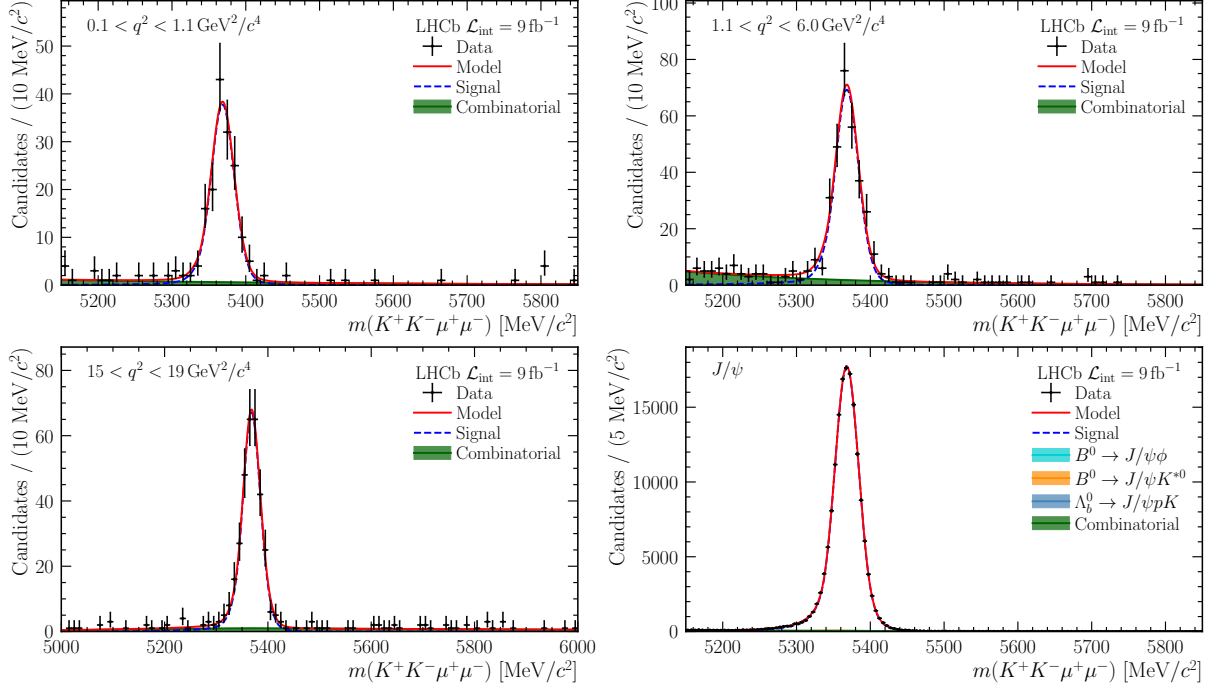


Figure 3: Mass distributions of selected $B_s^0 \rightarrow \phi\mu^+\mu^-$ candidates in the (top left) low-, (top right) central-, (bottom left) high- q^2 , and (bottom right) J/ψ bins. The data are summed over the three run periods and are compared with the result of the fit described in the text.

References

- [1] CDF collaboration, T. Aaltonen *et al.*, *Observation of the baryonic flavor-changing neutral current decay $\Lambda_b \rightarrow \Lambda\mu^+\mu^-$* , *Phys. Rev. Lett.* **107** (2011) 201802, [arXiv:1107.3753](#).
- [2] LHCb collaboration, R. Aaij *et al.*, *Differential branching fraction and angular analysis of the decay $B_s^0 \rightarrow \phi\mu^+\mu^-$* , *JHEP* **07** (2013) 084, [arXiv:1305.2168](#).
- [3] LHCb collaboration, R. Aaij *et al.*, *Angular analysis and differential branching fraction of the decay $B_s^0 \rightarrow \phi\mu^+\mu^-$* , *JHEP* **09** (2015) 179, [arXiv:1506.08777](#).
- [4] LHCb collaboration, R. Aaij *et al.*, *Branching fraction measurements of the rare $B_s^0 \rightarrow \phi\mu^+\mu^-$ and $B_s^0 \rightarrow f_2'(1525)\mu^+\mu^-$ decays*, *Phys. Rev. Lett.* **127** (2021) 151801, [arXiv:2105.14007](#).
- [5] R. R. Horgan, Z. Liu, S. Meinel, and M. Wingate, *Lattice QCD calculation of form factors describing the rare decays $B \rightarrow K^*\ell^+\ell^-$ and $B_s \rightarrow \phi\ell^+\ell^-$* , *Phys. Rev.* **D89** (2014) 094501, [arXiv:1310.3722](#).
- [6] A. Bharucha, D. M. Straub, and R. Zwicky, *$B \rightarrow V\ell^+\ell^-$ in the Standard Model from light-cone sum rules*, *JHEP* **08** (2016) 098, [arXiv:1503.05534](#).
- [7] M. Ciuchini *et al.*, *$B \rightarrow K^*\ell^+\ell^-$ decays at large recoil in the Standard Model: a theoretical reappraisal*, *JHEP* **06** (2016) 116, [arXiv:1512.07157](#).
- [8] N. Gubernari, M. Reboud, D. van Dyk, and J. Virto, *Improved theory predictions and global analysis of exclusive $b \rightarrow s\mu^+\mu^-$ processes*, *JHEP* **09** (2022) 133, [arXiv:2206.03797](#).
- [9] LHCb collaboration, R. Aaij *et al.*, *Angular analysis of the rare decay $B_s^0 \rightarrow \phi\mu^+\mu^-$* , *JHEP* **11** (2021) 043, [arXiv:2107.13428](#).
- [10] LHCb collaboration, R. Aaij *et al.*, *Differential branching fractions and isospin asymmetries of $B \rightarrow K^{(*)}\mu^+\mu^-$ decays*, *JHEP* **06** (2014) 133, [arXiv:1403.8044](#).
- [11] CMS collaboration, A. M. Sirunyan *et al.*, *Measurement of angular parameters from the decay $B^0 \rightarrow K^{*0}\mu^+\mu^-$ in proton-proton collisions at $\sqrt{s} = 8$ TeV*, *Phys. Lett.* **B781** (2018) 517, [arXiv:1710.02846](#).
- [12] ATLAS collaboration, M. Aaboud *et al.*, *Angular analysis of $B_d^0 \rightarrow K^*\mu^+\mu^-$ decays in pp collisions at $\sqrt{s} = 8$ TeV with the ATLAS detector*, *JHEP* **10** (2018) 047, [arXiv:1805.04000](#).
- [13] LHCb collaboration, R. Aaij *et al.*, *Measurement of CP-averaged observables in the $B^0 \rightarrow K^{*0}\mu^+\mu^-$ decay*, *Phys. Rev. Lett.* **125** (2020) 011802, [arXiv:2003.04831](#).
- [14] LHCb collaboration, R. Aaij *et al.*, *Angular analysis of the $B^+ \rightarrow K^{*+}\mu^+\mu^-$ decay*, *Phys. Rev. Lett.* **126** (2021) 161802, [arXiv:2012.13241](#).
- [15] LHCb collaboration, R. Aaij *et al.*, *Amplitude analysis of the $B^0 \rightarrow K^{*0}\mu^+\mu^-$ decay*, *Phys. Rev. Lett.* **132** (2024) 131801, [arXiv:2312.09115](#).

- [16] LHCb collaboration, R. Aaij *et al.*, *Comprehensive analysis of local and nonlocal amplitudes in the $B^0 \rightarrow K^{*0}\mu^+\mu^-$ decay*, *JHEP* **09** (2024) 026, [arXiv:2405.17347](#).
- [17] CMS collaboration, A. Hayrapetyan *et al.*, *Test of lepton flavor universality in $B^\pm \rightarrow K^\pm\mu^+\mu^-$ and $B^\pm \rightarrow K^\pm e^+e^-$ decays in proton-proton collisions at $\sqrt{s} = 13$ TeV*, [arXiv:2401.07090](#).
- [18] CMS collaboration, *Angular analysis of the $B^0 \rightarrow K^{*0}(892)\mu^+\mu^-$ decay at $\sqrt{s} = 13$ TeV*, [CMS-PAS-BPH-21-002](#), 2024.
- [19] A. Crivellin and B. Mellado, *Anomalies in particle physics and their implications for physics beyond the standard model*, *Nature Rev. Phys.* **6** (2024) 294, [arXiv:2309.03870](#).
- [20] B. Capdevila, A. Crivellin, and J. Matias, *Review of semileptonic B anomalies*, *Eur. Phys. J. ST* **1** (2023) 20, [arXiv:2309.01311](#).
- [21] P. Athron, R. Martinez, and C. Sierra, *B meson anomalies and large $B^+ \rightarrow K^+\nu\bar{\nu}$ in non-universal $U(1)'$ models*, *JHEP* **02** (2024) 121, [arXiv:2308.13426](#).
- [22] B. Allanach and A. Mullin, *Plan B: new Z' models for $b \rightarrow s\ell^+\ell^-$ anomalies*, *JHEP* **09** (2023) 173, [arXiv:2306.08669](#).
- [23] J. Davighi and B. A. Stefanek, *Deconstructed hypercharge: a natural model of flavour*, *JHEP* **11** (2023) 100, [arXiv:2305.16280](#).
- [24] G. Isidori, Z. Polonsky, and A. Tinari, *Semi-inclusive $b \rightarrow s\bar{\ell}\ell$ transitions at high q^2* , *Phys. Rev.* **D108** (2023) 093008, [arXiv:2305.03076](#).
- [25] M. Ciuchini *et al.*, *Constraints on lepton universality violation from rare B decays*, *Phys. Rev.* **D107** (2023) 055036, [arXiv:2212.10516](#).
- [26] A. Greljo, J. Salko, A. Smolkovič, and P. Stangl, *Rare b decays meet high-mass Drell-Yan*, *JHEP* **05** (2023) 087, [arXiv:2212.10497](#).
- [27] N. R. Singh Chundawat, *CP violation in $b \rightarrow s\ell\ell$: a model independent analysis*, *Phys. Rev.* **D107** (2023) 075014, [arXiv:2207.10613](#).
- [28] HPQCD collaboration, W. G. Parrott, C. Bouchard, and C. T. H. Davies, *Standard Model predictions for $B \rightarrow K\ell^+\ell^-$, $B \rightarrow K\ell_1^-\ell_2^+$ and $B \rightarrow K\nu\bar{\nu}$ using form factors from $N_f=2+1+1$ lattice QCD*, *Phys. Rev.* **D107** (2023) 014511, Erratum *ibid.* **D107** (2023) 119903, [arXiv:2207.13371](#).
- [29] M. Fernández Navarro and S. F. King, *B-anomalies in a twin Pati-Salam theory of flavour including the 2022 LHCb $R_{K^{(*)}}$ analysis*, *JHEP* **02** (2023) 188, [arXiv:2209.00276](#).
- [30] N. R. Singh Chundawat, *New physics in $B \rightarrow K^*\tau^+\tau^-$: A model independent analysis*, *Phys. Rev.* **D107** (2023) 055004, [arXiv:2212.01229](#).
- [31] B. Allanach and J. Davighi, *The Rumble in the Meson: a leptoquark versus a Z' to fit $b \rightarrow s\mu^+\mu^-$ anomalies including 2022 LHCb $R_{K^{(*)}}$ measurements*, *JHEP* **04** (2023) 033, [arXiv:2211.11766](#).

- [32] R. Bause, H. Gisbert, M. Golz, and G. Hiller, *Model-independent analysis of $b \rightarrow d$ processes*, *Eur. Phys. J.* **C83** (2023) 419, [arXiv:2209.04457](#).
- [33] M. Ciuchini *et al.*, *Charming penguins and lepton universality violation in $b \rightarrow sl^+\ell^-$ decays*, *Eur. Phys. J.* **C83** (2023) 64, [arXiv:2110.10126](#).
- [34] M. Algueró *et al.*, *To $(b)e$ or not to $(b)e$: no electrons at LHCb*, *Eur. Phys. J.* **C83** (2023) 648, [arXiv:2304.07330](#).
- [35] M. Bordone, G. Isidori, and A. Pattori, *On the Standard Model predictions for R_K and R_{K^*}* , *Eur. Phys. J.* **C76** (2016) 440, [arXiv:1605.07633](#).
- [36] G. Isidori, D. Lancierini, S. Nabeebaccus, and R. Zwicky, *QED in $\bar{B} \rightarrow \bar{K}l^+\ell^-$ LFU ratios: theory versus experiment, a Monte Carlo study*, *JHEP* **10** (2022) 146, [arXiv:2205.08635](#).
- [37] G. Hiller and F. Kruger, *More model-independent analysis of $b \rightarrow s$ processes*, *Phys. Rev.* **D69** (2004) 074020, [arXiv:hep-ph/0310219](#).
- [38] S. L. Glashow, D. Guadagnoli, and K. Lane, *Lepton flavor violation in B decays?*, *Phys. Rev. Lett.* **114** (2015) 091801, [arXiv:1411.0565](#).
- [39] I. Doršner *et al.*, *Physics of leptoquarks in precision experiments and at particle colliders*, *Phys. Rept.* **641** (2016) 1, [arXiv:1603.04993](#).
- [40] D. Buttazzo, A. Greljo, G. Isidori, and D. Marzocca, *B -physics anomalies: a guide to combined explanations*, *JHEP* **11** (2017) 044, [arXiv:1706.07808](#).
- [41] BaBar collaboration, J. P. Lees *et al.*, *Measurement of branching fractions and rate asymmetries in the rare decays $B \rightarrow K^{(*)}l^+\ell^-$* , *Phys. Rev.* **D86** (2012) 032012, [arXiv:1204.3933](#).
- [42] Belle collaboration, S. Choudhury *et al.*, *Test of lepton flavor universality and search for lepton flavor violation in $B \rightarrow K\ell\ell$ decays*, *JHEP* **03** (2021) 105, [arXiv:1908.01848](#).
- [43] LHCb collaboration, R. Aaij *et al.*, *Test of lepton universality using $B^+ \rightarrow K^+l^+\ell^-$ decays*, *Phys. Rev. Lett.* **113** (2014) 151601, [arXiv:1406.6482](#).
- [44] LHCb collaboration, R. Aaij *et al.*, *Test of lepton universality with $B^0 \rightarrow K^{*0}l^+\ell^-$ decays*, *JHEP* **08** (2017) 055, [arXiv:1705.05802](#).
- [45] LHCb collaboration, R. Aaij *et al.*, *Test of lepton universality using $\Lambda_b^0 \rightarrow pK^-l^+\ell^-$ decays*, *JHEP* **05** (2020) 040, [arXiv:1912.08139](#).
- [46] LHCb collaboration, R. Aaij *et al.*, *Test of lepton universality in beauty-quark decays*, *Nature Physics* **18** (2022) 277, [arXiv:2103.11769](#).
- [47] LHCb collaboration, R. Aaij *et al.*, *Tests of lepton universality using $B^0 \rightarrow K_S^0l^+\ell^-$ and $B^+ \rightarrow K^{*+}l^+\ell^-$ decays*, *Phys. Rev. Lett.* **128** (2022) 191802, [arXiv:2110.09501](#).

- [48] LHCb collaboration, R. Aaij *et al.*, *Measurement of lepton universality parameters in $B^+ \rightarrow K^+\ell^+\ell^-$ and $B^0 \rightarrow K^{*0}\ell^+\ell^-$ decays*, *Phys. Rev.* **D108** (2023) 032002, [arXiv:2212.09153](#).
- [49] LHCb collaboration, R. Aaij *et al.*, *Test of lepton universality in $b \rightarrow s\ell^+\ell^-$ decays*, *Phys. Rev. Lett.* **131** (2023) 051803, [arXiv:2212.09152](#).
- [50] LHCb collaboration, A. A. Alves Jr. *et al.*, *The LHCb detector at the LHC*, *JINST* **3** (2008) S08005.
- [51] LHCb collaboration, R. Aaij *et al.*, *LHCb detector performance*, *Int. J. Mod. Phys.* **A30** (2015) 1530022, [arXiv:1412.6352](#).
- [52] R. Aaij *et al.*, *Performance of the LHCb Vertex Locator*, *JINST* **9** (2014) P09007, [arXiv:1405.7808](#).
- [53] R. Arink *et al.*, *Performance of the LHCb Outer Tracker*, *JINST* **9** (2014) P01002, [arXiv:1311.3893](#).
- [54] P. d'Argent *et al.*, *Improved performance of the LHCb Outer Tracker in LHC Run 2*, *JINST* **12** (2017) P11016, [arXiv:1708.00819](#).
- [55] M. Adinolfi *et al.*, *Performance of the LHCb RICH detector at the LHC*, *Eur. Phys. J.* **C73** (2013) 2431, [arXiv:1211.6759](#).
- [56] A. A. Alves Jr. *et al.*, *Performance of the LHCb muon system*, *JINST* **8** (2013) P02022, [arXiv:1211.1346](#).
- [57] R. Aaij *et al.*, *The LHCb trigger and its performance in 2011*, *JINST* **8** (2013) P04022, [arXiv:1211.3055](#).
- [58] T. Sjöstrand, S. Mrenna, and P. Skands, *A brief introduction to PYTHIA 8.1*, *Comput. Phys. Commun.* **178** (2008) 852, [arXiv:0710.3820](#); T. Sjöstrand, S. Mrenna, and P. Skands, *PYTHIA 6.4 physics and manual*, *JHEP* **05** (2006) 026, [arXiv:hep-ph/0603175](#).
- [59] I. Belyaev *et al.*, *Handling of the generation of primary events in Gauss, the LHCb simulation framework*, *J. Phys. Conf. Ser.* **331** (2011) 032047.
- [60] D. J. Lange, *The EvtGen particle decay simulation package*, *Nucl. Instrum. Meth.* **A462** (2001) 152.
- [61] N. Davidson, T. Przedzinski, and Z. Was, *PHOTOS interface in C++: Technical and physics documentation*, *Comp. Phys. Comm.* **199** (2016) 86, [arXiv:1011.0937](#).
- [62] A. Ali, P. Ball, L. T. Handoko, and G. Hiller, *Comparative study of the decays $B \rightarrow (K, K^*)\ell^+\ell^-$ in standard model and supersymmetric theories*, *Phys. Rev.* **D61** (2000) 074024, [arXiv:hep-ph/9910221](#).
- [63] S. Descotes-Genon and J. Virto, *Time dependence in $B \rightarrow V\ell\ell$ decays*, *JHEP* **04** (2015) 045, Erratum *ibid.* **07** (2015) 049, [arXiv:1502.05509](#).

- [64] P. Ball and R. Zwicky, $B_{d,s} \rightarrow \rho, \omega, K^*, \phi$ decay form-factors from light-cone sum rules revisited, *Phys. Rev.* **D71** (2005) 014029, [arXiv:hep-ph/0412079](#).
- [65] Geant4 collaboration, J. Allison *et al.*, *Geant4 developments and applications*, *IEEE Trans. Nucl. Sci.* **53** (2006) 270; Geant4 collaboration, S. Agostinelli *et al.*, *Geant4: A simulation toolkit*, *Nucl. Instrum. Meth.* **A506** (2003) 250.
- [66] M. Clemencic *et al.*, *The LHCb simulation application, Gauss: Design, evolution and experience*, *J. Phys. Conf. Ser.* **331** (2011) 032023.
- [67] V. V. Gligorov and M. Williams, *Efficient, reliable and fast high-level triggering using a bonsai boosted decision tree*, *JINST* **8** (2013) P02013, [arXiv:1210.6861](#).
- [68] T. Likhomanenko *et al.*, *LHCb topological trigger reoptimization*, *J. Phys. Conf. Ser.* **664** (2015) 082025, [arXiv:1510.00572](#).
- [69] Particle Data Group, S. Navas *et al.*, *Review of particle physics*, *Phys. Rev.* **D110** (2024) 030001.
- [70] A. V. Dorogush, V. Ershov, and A. Gulin, *Catboost: gradient boosting with categorical features support*, [arXiv:1810.11363](#).
- [71] A. Blum, A. Kalai, and J. Langford, *Beating the hold-out: bounds for k -fold and progressive cross-validation*, in *Proceedings of the Twelfth Annual Conference on Computational Learning Theory, COLT '99, (New York, NY, USA), 203–208*, Association for Computing Machinery, 1999.
- [72] J. Eschle, A. Puig Navarro, R. Silva Coutinho, and N. Serra, *zfit: Scalable pythonic fitting*, *SoftwareX* **11** (2020) 100508.
- [73] N. L. Johnson, *Systems of frequency curves generated by methods of translation*, *Biometrika* **36** (1949) 149.
- [74] S. S. Wilks, *The large-sample distribution of the likelihood ratio for testing composite hypotheses*, *Ann. Math. Stat.* **9** (1938) 60.
- [75] LHCb collaboration, R. Aaij *et al.*, *Measurements of the branching fraction ratio $\mathcal{B}(\phi \rightarrow \mu^+\mu^-)/\mathcal{B}(\phi \rightarrow e^+e^-)$ with charm meson decays*, *JHEP* **05** (2024) 293, [arXiv:2402.01336](#).
- [76] B. Efron, *Bootstrap methods: Another look at the jackknife*, *Ann. Statist.* **7** (1979) 1.
- [77] D. M. Straub, *flavio: a Python package for flavour and precision phenomenology in the Standard Model and beyond*, [arXiv:1810.08132](#).
- [78] LHCb collaboration, R. Aaij *et al.*, *Precise measurement of the f_s/f_d ratio of fragmentation fractions and of B_s^0 decay branching fractions*, *Phys. Rev.* **D104** (2021) 032005, [arXiv:2103.06810](#).
- [79] LHCb collaboration, R. Aaij *et al.*, *Constraints on the photon polarisation in $b \rightarrow s\gamma$ transitions using $B_s^0 \rightarrow \phi e^+e^-$ decays*, LHCb-PAPER-2024-030, in preparation, to be submitted to JHEP.

G. Tonani^{30,n,49} , X. Tong⁶ , D. Torres Machado² , L. Toscano¹⁹ , D.Y. Tou^{4,b} ,
C. Tripp¹⁴⁵ , G. Tuci²² , N. Tuning³⁸ , L.H. Uecker²² , A. Ukleja⁴⁰ ,
D.J. Unverzagt²² , B. Urbach⁵⁹ , E. Ursov⁴⁴ , A. Usachov³⁹ , A. Ustyuzhanin⁴⁴ ,
U. Uwer²² , V. Vagnoni²⁵ , V. Valcarce Cadenas⁴⁷ , G. Valenti²⁵ , N. Valls Canudas⁴⁹ ,
H. Van Hecke⁶⁸ , E. van Herwijnen⁶² , C.B. Van Hulse^{47,x} , R. Van Laak⁵⁰ ,
M. van Veghel³⁸ , G. Vasquez⁵¹ , R. Vazquez Gomez⁴⁶ , P. Vazquez Regueiro⁴⁷ ,
C. Vázquez Sierra⁴⁷ , S. Vecchi²⁶ , J.J. Velthuis⁵⁵ , M. Veltri^{27,w} ,
A. Venkateswaran⁵⁰ , M. Verdognia³² , M. Vesterinen⁵⁷ , D. Vico Benet⁶⁴ , P.
Vidrier Villalba⁴⁶ , M. Vieites Diaz⁴⁹ , X. Vilasis-Cardona⁴⁵ , E. Vilella Figueras⁶¹ ,
A. Villa²⁵ , P. Vincent¹⁶ , F.C. Volle⁵⁴ , D. vom Bruch¹³ , N. Voropaev⁴⁴ , K. Vos⁷⁹ ,
G. Vouters¹⁰ , C. Vrahas⁵⁹ , J. Wagner¹⁹ , J. Walsh³⁵ , E.J. Walton^{1,57} , G. Wan⁶ ,
C. Wang²² , G. Wang⁸ , J. Wang⁶ , J. Wang⁵ , J. Wang^{4,b} , J. Wang⁷⁴ ,
M. Wang³⁰ , N. W. Wang⁷ , R. Wang⁵⁵ , X. Wang⁸ , X. Wang⁷² , X. W. Wang⁶² ,
Y. Wang⁶ , Z. Wang¹⁴ , Z. Wang^{4,b} , Z. Wang³⁰ , J.A. Ward^{57,1} , M. Waterlaet⁴⁹ ,
N.K. Watson⁵⁴ , D. Websdale⁶² , Y. Wei⁶ , J. Wendel⁸¹ , B.D.C. Westhenry⁵⁵ ,
C. White⁵⁶ , M. Whitehead⁶⁰ , E. Whiter⁵⁴ , A.R. Wiederhold⁶³ , D. Wiedner¹⁹ ,
G. Wilkinson⁶⁴ , M.K. Wilkinson⁶⁶ , M. Williams⁶⁵ , M. J. Williams⁴⁹ ,
M.R.J. Williams⁵⁹ , R. Williams⁵⁶ , Z. Williams⁵⁵ , F.F. Wilson⁵⁸ , M. Winn¹² ,
W. Wislicki⁴² , M. Witek⁴¹ , L. Witola²² , G. Wormser¹⁴ , S.A. Wotton⁵⁶ , H. Wu⁶⁹ ,
J. Wu⁸ , X. Wu⁷⁴ , Y. Wu⁶ , Z. Wu⁷ , K. Wyllie⁴⁹ , S. Xian⁷² , Z. Xiang⁵ , Y. Xie⁸ ,
A. Xu³⁵ , J. Xu⁷ , L. Xu^{4,b} , L. Xu^{4,b} , M. Xu⁵⁷ , Z. Xu⁴⁹ , Z. Xu⁷ , Z. Xu⁵ ,
D. Yang⁴ , K. Yang⁶² , S. Yang⁷ , X. Yang⁶ , Y. Yang^{29,m} , Z. Yang⁶ , Z. Yang⁶⁷ ,
V. Yeroshenko¹⁴ , H. Yeung⁶³ , H. Yin⁸ , X. Yin⁷ , C. Y. Yu⁶ , J. Yu⁷¹ ,
X. Yuan⁵ , Y. Yuan^{5,7} , E. Zaffaroni⁵⁰ , M. Zavertyaev²¹ , M. Zdybal⁴¹ ,
F. Zenesini^{25,j} , C. Zeng^{5,7} , M. Zeng^{4,b} , C. Zhang⁶ , D. Zhang⁸ , J. Zhang⁷ ,
L. Zhang^{4,b} , S. Zhang⁷¹ , S. Zhang⁶⁴ , Y. Zhang⁶ , Y. Z. Zhang^{4,b} , Y. Zhao²² ,
A. Zharkova⁴⁴ , A. Zhelezov²² , S. Z. Zheng⁶ , X. Z. Zheng^{4,b} , Y. Zheng⁷ ,
T. Zhou⁶ , X. Zhou⁸ , Y. Zhou⁷ , V. Zhovkovska⁵⁷ , L. Z. Zhu⁷ , X. Zhu^{4,b} ,
X. Zhu⁸ , V. Zhukov¹⁷ , J. Zhuo⁴⁸ , Q. Zou^{5,7} , D. Zuliani^{33,p} , G. Zunica⁵⁰ .

¹*School of Physics and Astronomy, Monash University, Melbourne, Australia*

²*Centro Brasileiro de Pesquisas Físicas (CBPF), Rio de Janeiro, Brazil*

³*Universidade Federal do Rio de Janeiro (UFRJ), Rio de Janeiro, Brazil*

⁴*Department of Engineering Physics, Tsinghua University, Beijing, China, Beijing, China*

⁵*Institute Of High Energy Physics (IHEP), Beijing, China*

⁶*School of Physics State Key Laboratory of Nuclear Physics and Technology, Peking University, Beijing, China*

⁷*University of Chinese Academy of Sciences, Beijing, China*

⁸*Institute of Particle Physics, Central China Normal University, Wuhan, Hubei, China*

⁹*Consejo Nacional de Rectores (CONARE), San Jose, Costa Rica*

¹⁰*Université Savoie Mont Blanc, CNRS, IN2P3-LAPP, Annecy, France*

¹¹*Université Clermont Auvergne, CNRS/IN2P3, LPC, Clermont-Ferrand, France*

¹²*Université Paris-Saclay, Centre d'Etudes de Saclay (CEA), IRFU, Saclay, France, Gif-Sur-Yvette, France*

¹³*Aix Marseille Univ, CNRS/IN2P3, CPPM, Marseille, France*

¹⁴*Université Paris-Saclay, CNRS/IN2P3, IJCLab, Orsay, France*

¹⁵*Laboratoire Leprince-Ringuet, CNRS/IN2P3, Ecole Polytechnique, Institut Polytechnique de Paris, Palaiseau, France*

¹⁶*LPNHE, Sorbonne Université, Paris Diderot Sorbonne Paris Cité, CNRS/IN2P3, Paris, France*

¹⁷*I. Physikalisches Institut, RWTH Aachen University, Aachen, Germany*

¹⁸*Universität Bonn - Helmholtz-Institut für Strahlen und Kernphysik, Bonn, Germany*

¹⁹*Fakultät Physik, Technische Universität Dortmund, Dortmund, Germany*

²⁰*Physikalisches Institut, Albert-Ludwigs-Universität Freiburg, Freiburg, Germany*

- ²¹ *Max-Planck-Institut für Kernphysik (MPIK), Heidelberg, Germany*
- ²² *Physikalisches Institut, Ruprecht-Karls-Universität Heidelberg, Heidelberg, Germany*
- ²³ *School of Physics, University College Dublin, Dublin, Ireland*
- ²⁴ *INFN Sezione di Bari, Bari, Italy*
- ²⁵ *INFN Sezione di Bologna, Bologna, Italy*
- ²⁶ *INFN Sezione di Ferrara, Ferrara, Italy*
- ²⁷ *INFN Sezione di Firenze, Firenze, Italy*
- ²⁸ *INFN Laboratori Nazionali di Frascati, Frascati, Italy*
- ²⁹ *INFN Sezione di Genova, Genova, Italy*
- ³⁰ *INFN Sezione di Milano, Milano, Italy*
- ³¹ *INFN Sezione di Milano-Bicocca, Milano, Italy*
- ³² *INFN Sezione di Cagliari, Monserrato, Italy*
- ³³ *INFN Sezione di Padova, Padova, Italy*
- ³⁴ *INFN Sezione di Perugia, Perugia, Italy*
- ³⁵ *INFN Sezione di Pisa, Pisa, Italy*
- ³⁶ *INFN Sezione di Roma La Sapienza, Roma, Italy*
- ³⁷ *INFN Sezione di Roma Tor Vergata, Roma, Italy*
- ³⁸ *Nikhef National Institute for Subatomic Physics, Amsterdam, Netherlands*
- ³⁹ *Nikhef National Institute for Subatomic Physics and VU University Amsterdam, Amsterdam, Netherlands*
- ⁴⁰ *AGH - University of Krakow, Faculty of Physics and Applied Computer Science, Kraków, Poland*
- ⁴¹ *Henryk Niewodniczanski Institute of Nuclear Physics Polish Academy of Sciences, Kraków, Poland*
- ⁴² *National Center for Nuclear Research (NCBJ), Warsaw, Poland*
- ⁴³ *Horia Hulubei National Institute of Physics and Nuclear Engineering, Bucharest-Magurele, Romania*
- ⁴⁴ *Affiliated with an institute covered by a cooperation agreement with CERN*
- ⁴⁵ *DS4DS, La Salle, Universitat Ramon Llull, Barcelona, Spain*
- ⁴⁶ *ICCUB, Universitat de Barcelona, Barcelona, Spain*
- ⁴⁷ *Instituto Galego de Física de Altas Enerxías (IGFAE), Universidade de Santiago de Compostela, Santiago de Compostela, Spain*
- ⁴⁸ *Instituto de Física Corpuscular, Centro Mixto Universidad de Valencia - CSIC, Valencia, Spain*
- ⁴⁹ *European Organization for Nuclear Research (CERN), Geneva, Switzerland*
- ⁵⁰ *Institute of Physics, Ecole Polytechnique Fédérale de Lausanne (EPFL), Lausanne, Switzerland*
- ⁵¹ *Physik-Institut, Universität Zürich, Zürich, Switzerland*
- ⁵² *NSC Kharkiv Institute of Physics and Technology (NSC KIPT), Kharkiv, Ukraine*
- ⁵³ *Institute for Nuclear Research of the National Academy of Sciences (KINR), Kyiv, Ukraine*
- ⁵⁴ *School of Physics and Astronomy, University of Birmingham, Birmingham, United Kingdom*
- ⁵⁵ *H.H. Wills Physics Laboratory, University of Bristol, Bristol, United Kingdom*
- ⁵⁶ *Cavendish Laboratory, University of Cambridge, Cambridge, United Kingdom*
- ⁵⁷ *Department of Physics, University of Warwick, Coventry, United Kingdom*
- ⁵⁸ *STFC Rutherford Appleton Laboratory, Didcot, United Kingdom*
- ⁵⁹ *School of Physics and Astronomy, University of Edinburgh, Edinburgh, United Kingdom*
- ⁶⁰ *School of Physics and Astronomy, University of Glasgow, Glasgow, United Kingdom*
- ⁶¹ *Oliver Lodge Laboratory, University of Liverpool, Liverpool, United Kingdom*
- ⁶² *Imperial College London, London, United Kingdom*
- ⁶³ *Department of Physics and Astronomy, University of Manchester, Manchester, United Kingdom*
- ⁶⁴ *Department of Physics, University of Oxford, Oxford, United Kingdom*
- ⁶⁵ *Massachusetts Institute of Technology, Cambridge, MA, United States*
- ⁶⁶ *University of Cincinnati, Cincinnati, OH, United States*
- ⁶⁷ *University of Maryland, College Park, MD, United States*
- ⁶⁸ *Los Alamos National Laboratory (LANL), Los Alamos, NM, United States*
- ⁶⁹ *Syracuse University, Syracuse, NY, United States*
- ⁷⁰ *Pontifícia Universidade Católica do Rio de Janeiro (PUC-Rio), Rio de Janeiro, Brazil, associated to ³*
- ⁷¹ *School of Physics and Electronics, Hunan University, Changsha City, China, associated to ⁸*
- ⁷² *Guangdong Provincial Key Laboratory of Nuclear Science, Guangdong-Hong Kong Joint Laboratory of Quantum Matter, Institute of Quantum Matter, South China Normal University, Guangzhou, China, associated to ⁴*

- ⁷³ Lanzhou University, Lanzhou, China, associated to ⁵
⁷⁴ School of Physics and Technology, Wuhan University, Wuhan, China, associated to ⁴
⁷⁵ Departamento de Física, Universidad Nacional de Colombia, Bogota, Colombia, associated to ¹⁶
⁷⁶ Ruhr Universitaet Bochum, Fakultaet f. Physik und Astronomie, Bochum, Germany, associated to ¹⁹
⁷⁷ Eotvos Lorand University, Budapest, Hungary, associated to ⁴⁹
⁷⁸ Van Swinderen Institute, University of Groningen, Groningen, Netherlands, associated to ³⁸
⁷⁹ Universiteit Maastricht, Maastricht, Netherlands, associated to ³⁸
⁸⁰ Tadeusz Kosciuszko Cracow University of Technology, Cracow, Poland, associated to ⁴¹
⁸¹ Universidad de Coruña, A Coruña, Spain, associated to ⁴⁵
⁸² Department of Physics and Astronomy, Uppsala University, Uppsala, Sweden, associated to ⁶⁰
⁸³ University of Michigan, Ann Arbor, MI, United States, associated to ⁶⁹

^a Centro Federal de Educação Tecnológica Celso Suckow da Fonseca, Rio De Janeiro, Brazil

^b Center for High Energy Physics, Tsinghua University, Beijing, China

^c Hangzhou Institute for Advanced Study, UCAS, Hangzhou, China

^d School of Physics and Electronics, Henan University, Kaifeng, China

^e LIP6, Sorbonne Université, Paris, France

^f Lamarr Institute for Machine Learning and Artificial Intelligence, Dortmund, Germany

^g Universidad Nacional Autónoma de Honduras, Tegucigalpa, Honduras

^h Università di Bari, Bari, Italy

ⁱ Università di Bergamo, Bergamo, Italy

^j Università di Bologna, Bologna, Italy

^k Università di Cagliari, Cagliari, Italy

^l Università di Ferrara, Ferrara, Italy

^m Università di Genova, Genova, Italy

ⁿ Università degli Studi di Milano, Milano, Italy

^o Università degli Studi di Milano-Bicocca, Milano, Italy

^p Università di Padova, Padova, Italy

^q Università di Perugia, Perugia, Italy

^r Scuola Normale Superiore, Pisa, Italy

^s Università di Pisa, Pisa, Italy

^t Università della Basilicata, Potenza, Italy

^u Università di Roma Tor Vergata, Roma, Italy

^v Università di Siena, Siena, Italy

^w Università di Urbino, Urbino, Italy

^x Universidad de Alcalá, Alcalá de Henares, Spain

^y Facultad de Ciencias Físicas, Madrid, Spain

^z Department of Physics/Division of Particle Physics, Lund, Sweden

† Deceased